Probing Ca^{2+}-Induced Conformational Changes in Porcine Calmodulin by H/D Exchange and ESI-MS: Effect of Cations and Ionic Strength†

Mei M. Zhu, Don L. Rempel, Jiang Zhao,‡ Daryl E. Giblin, and Michael L. Gross*

Department of Chemistry, Washington University, St. Louis, Missouri 63130

Received July 8, 2003; Revised Manuscript Received October 16, 2003

ABSTRACT: We applied a new method, "protein−ligand interaction using mass spectrometry, titration, and H/D exchange" (PLIMSTEX) [Zhu, M. M. (2003) *J. Am. Chem. Soc. 125,* 5252−5253], to determine the conformational changes, binding stoichiometry, and binding constants for Ca^{2+} interactions with calmodulin (CaM) under varying conditions of electrolyte identity and ionic strength. The outcome shows that CaM becomes less solvent-accessible and more compact upon Ca^{2+}-binding, as revealed by the PLIMSTEX curve. The formation of CaM−4Ca species is the biggest contributor to the shape of the titration curve, indicating that the formation of this species accounts for the largest conformational change in the stepwise Ca^{2+} binding. The Ca^{2+}-binding constants, when comparisons permit, agree with those in the literature within a factor of 3. The binding is influenced by ionic strength and the presence of other cations, although many of these cations do not cause conformational change in apo-CaM. Furthermore, Ca^{2+}-saturated CaM exhibits larger protection and higher Ca^{2+} affinity in media of low rather than high ionic strength. Both Ca^{2+} and Mg^{2+} bind to CaM with different affinities, causing different conformational changes. K^+, if it does bind, causes no detectable conformational change, and interactions of Ca^{2+} with CaM in the presence of Li^+, Na^+, and K^+ occur with similar affinities and associated changes in solvent accessibility. These metal ion effects point to nonspecific rather than competitive binding of alkali-metal ions. The rates of deuterium uptake by the various CaM−*x*Ca species follow a three-group (fast, intermediate, slow), pseudo-first-order kinetics model. Calcium binding causes the number of amide hydrogens to shift from the fast to the slow group. The results taken together not only provide new insight into CaM but also indicate that both PLIMSTEX and kinetic modeling of H/D exchange data may become general methods for probing protein conformations and quantifying protein−ligand interactions.

We describe in this paper the application of H/D[1] exchange combined with mass spectrometry (*1*−*5*) for determining the conformational changes induced by metal ion binding to a protein. We chose calmodulin (CaM) binding to Ca^{2+} as a template for the development of mass spectrometry in this area. Time-dependent changes of both the average mass and the distribution of the masses during deuterium uptake by a protein may provide insight into its changes in structure (*6*). Several Ca^{2+}-binding proteins to which exchange was previously applied are human cardiac tropnin C (*7*) and recoverin (*8*). A refolding study of bovine lactalbumin in the presence and absence of Ca^{2+} (*9*) indicates that the rate of the refolding is faster and the amount of protection is higher in the presence of Ca^{2+} than in its absence.

CaM is a ubiquitous Ca^{2+}-binding protein and the primary intracellular calcium sensor in eukaryotic cells. When bound to Ca^{2+}, CaM changes conformation, enabling it to bind and activate target proteins (for reviews, see refs *10*−*19*). Holo-CaM is dumbbell-shaped with a central α-helix separating two domains, each containing two calcium-binding sites. Although the crystal structure of apo-CaM is not known, the solution-structure determination, by heteronuclear NMR (*20*−*22*), reveals that the two antiparallel helices in each EF-hand of apo-CaM become perpendicular upon Ca^{2+} binding. The resultant movement of the Ca^{2+}-binding loops may cause the α-helices to become tighter and less solvent-accessible (*23*). NMR also shows that Ca^{2+} binding leads to exposure of hydrophobic surfaces, promoting binding to targets. The region linking the domains is an imperfect helix in solution (*24*) and is more flexible than can be indicated by X-ray crystallography. Calcium binding lowers the Stokes radius (R_s) of CaM (*25*) and the isolated domains (*26*, *27*), also indicating that Ca^{2+}-saturated CaM folds to a more compact form.

Calcium ions bind to CaM in a sequential manner (*28*, *29*). The average binding constants for the two C-domain sites are 6−10 times greater than those for the N domain (*30*, *31*). The Ca^{2+}-binding affinity decreases with an increase in the concentration of other cations (*29*, *31*). Mg^{2+} binds preferentially to the N domain (*32*−*34*) with lower affinity and less attendant conformational change (*35*, *36*). The apparent Ca^{2+} affinity decreases at physiological [Mg^{2+}], indicating either a direct competition between Mg^{2+} and Ca^{2+}

† These studies were supported by the National Institutes of Health (Grant No. 2P41RR00954).

* To whom correspondence should be addressed. Phone: (314) 935-4814. Fax: (314) 935-7484. E-mail: mgross@wuchem.wustl.edu.

‡ Present address: ChemRx, South San Francisco, CA 94080.

[1] Abbreviations: H/D, hydrogen/deuterium; CaM, calmodulin; PLIMSTEX, quantification of protein−ligand interaction using mass spectrometry, titration, and H/D exchange; ESI-MS, electrospray ionization mass spectrometry; HEPES, (*N*-[2-hydroxyethyl)piperazine-*N*′-[2-ethanesulfonic acid]); av, average; dev, deviation; RMS, root mean square.

10.1021/bi035188o CCC: $25.00
Published on Web 12/03/2003

in the Ca^{2+}-binding loop (*37*) or allosteric effector status for Mg^{2+} (*34*). K^+ may also bind competitively to the Ca^{2+} site (*29*); that binding, however, does not alter the conformation, suggesting that the effect of K^+ is to screen electrostatic interactions or to change activity coefficients (*31*, *38*). Questions about the metal ion binding for CaM still remain. For example, there are large variations in the four macroscopic Ca^{2+}-binding constants possibly because measurements were by different methods under different conditions, leaving open questions of cooperativity between the two domains.

Past efforts on CaM illustrate convincingly that the complete understanding of protein structure and interactions requires many experimental methods. Many of the Ca^{2+}-binding properties of CaM are known from X-ray crystallography (*39*−*43*), NMR (*20*−*22*, *34*, *44*−*47*), fluorescence (*26*, *31*, *48*−*51*), proteolytic footprinting (*27*, *52*−*54*), circular dicroism (*30*, *32*, *49*, *55*, *56*), infrared spectroscopy (*57*), Raman spectroscopy (*35*), UV (*56*, *58*), atomic absorption (*29*, *59*), calorimetry (*33*, *60*−*62*), gel-permeation chromatography (*25*−*27*), ultracentrifugation (*56*, *63*, *64*), flow dialysis (*29*, *33*, *61*), rapid-density measurement (*65*), Ca-potential measurement (*59*, *66*, *67*), electron paramagnetic resonance (*36*), and mass spectrometry (MS) (*68*−*80*).

We reported in 1999 that the titration of CaM with Ca^{2+} is accompanied by a measurable change in the extent of H/D exchange (*23*) Since then, we have improved the experimental procedure, constructed a means to model the titration, and applied the combination to measure binding affinities of ligands (including metal ions) to proteins. We describe here the application of the improved methodology, which we call PLIMSTEX (protein−ligand interaction using mass spectrometry, titration, and H/D exchange) (*81*), and of a complementary kinetic approach to explore the effects of ionic strength and other cations on the Ca^{2+} affinity of CaM. This is the first reported application following the introduction of PLIMSTEX for determining affinity and conformational changes caused by protein−ligand interactions. We also describe the kinetic analysis, which implements a three-group, pseudo-first-order kinetics model to analyze changes in H/D exchange of CaM as a function of time and $[Ca^{2+}]$. The goals are not only to contribute to the substantial effort already made to understand CaM but also to test the methodology, which we expect will be ultimately sensitive, specific, fast, and convenient, as a tool in biophysical chemistry.

EXPERIMENTAL PROCEDURES

Materials. "Calcium-free" porcine calmodulin (MW 16790) was purchased from Ocean Biologics Co. (Edmonds, WA). Glass-distilled D_2O was obtained from Cambridge Isotope Laboratories, Inc. (Andover, MA). Deionized water (18.2 MΩ) was generated from a Millipore water filtering device (Bedford, MA). Other chemicals were obtained from Sigma-Aldrich (St. Louis, MO) at the highest purity available.

LC/ESI-MS with an Ion-Trap Mass Spectrometer. ESI mass spectra were obtained with a Finnigan Classic LCQ ion-trap mass spectrometer (San Jose, CA) with an electrospray-ionization source. The sample was loaded onto a Zorbax C-18 SBW column (10 mm × 0.32 mm i.d.; Microtech Scientific, Vista, CA) using a six-pore Rheodyne 7725 manual sample injector (Cobert Associates, St. Louis, MO). After manual desalting in the "load" mode, the injector was switched to the "inject" mode, and the protein was rapidly eluted to the mass spectrometer. HPLC was carried out using a Waters 600MS pump (Milford, MA) with an isocratic flow of 80% CH_3CN, 14.9% H_2O, and 5.1% CH_3COOH. The flow, split by a splitter (LC-packings, San Francisco, CA) at 10:1, was introduced to the column and then the mass spectrometer at a flow rate of 33 μL/min. The spray voltage was 5.0 kV, and the capillary temperature was 200 °C. All data were acquired in the positive-ion mode at unit mass resolving power between *m*/*z* 800 and *m*/*z* 2000. Normally 10 scans were averaged and processed using Finnigan Xcalibur 1.1 software. The raw data were transformed using Bioworks software from Finnigan. The mass centroids of the "deconvoluted" peaks were used for calculating the deuterium shift.

LC−ESI-MS with a Q-TOF Mass Spectrometer. To obtain better resolving power and a more accurate mass assignment, a Micromass Q-Tof Ultima GLOBAL mass spectrometer (Manchester, U.K.) with a Z-spray ESI source was used for some titrations. A solution of 80:19:1 (v/v/v) CH_3CN/H_2O/HCOOH was introduced into an Opti-Guard C18 column (10 mm × 1 mm i.d.; Cobert Associates) and then into the mass spectrometer at a flow rate of 32 μL/min using a Waters Cap-LC system. The capillary voltage was 3.4 kV, and the source and desolvation temperatures were 80 and 150 °C, respectively. The cone gas flow was 40 L/h, and the desolvation gas flow was 400 L/h. All data were acquired in the positive-ion mode by using the TOF at 10000 mass resolving power between *m*/*z* 800 and *m*/*z* 2000. Normally 10 scans were summed and processed using MassLynx 3.5. The molecular mass was determined using the maximum entropy algorithm (MaxEnt1 in MassLynx 3.5).

H/D Exchange Protocol. NH_4OAc solution was prepared by dissolving NH_4OAc in H_2O or D_2O. The pH was adjusted to 7.0 using NH_4OH or NH_4OD. HEPES buffer was prepared by mixing 50 mM HEPES acid and HEPES Na salt in H_2O or D_2O solutions (other salts were added to both solutions when needed), to give the final buffer solutions at an apparent pH of 7.4. All pH values reported here were the apparent pH measured directly using a glass electrode without further correction (*82*) for the D_2O solution or D_2O/H_2O exchange media. Apo-CaM stock solutions were prepared by dissolving lyophilized CaM in various aqueous buffer solutions to give 3 mM (for exchange at 99:1 D_2O/H_2O) or 200 μM (for exchange at 90:10 D_2O/H_2O). A Ca^{2+} stock solution was prepared by dissolving $CaCl_2$ in the same buffer/salt solutions to give 200 mM (for exchange in 99:1 D_2O/H_2O) or 40 mM (for exchange in 90:10 D_2O/H_2O). For the titration in NH_4OAc and HEPES/KNO_3 solutions, $Ca(OAc)_2$ or $Ca(NO_3)_2$ was used as the Ca^{2+} source. Individual Ca solutions used in each titration were prepared by diluting the stock Ca^{2+} with aqueous buffer. For Ca^{2+} titrations in 99:1 D_2O/H_2O, 1 μL of apo-CaM was incubated with 1 μL of $CaCl_2$ for 30 min, and 198 μL of D_2O (containing the same concentration of buffer and salt as the protein solution) was added to initiate H/D exchange. For Ca titrations in 90:10 D_2O/H_2O, 7.5 μL of apo-CaM was incubated with 2.5 μL of $CaCl_2$ for 30 min, and 90 μL of D_2O (with the same concentration of buffer and salt) was added to initiate the exchange.

Titrations with Mg^{2+} and K^+ were conducted in a similar way by replacing $CaCl_2$ with $MgCl_2$ or KCl, respectively.

Because the binding properties of these ions are different, the highest ligand total concentrations for Ca^{2+}, Mg^{2+}, and K^+ used in these H/D exchange titrations were 1, 100, and 300 mM, respectively. All incubations and H/D exchanges were carried out at room temperature (21.5−25 °C). The final concentration of CaM in H/D exchange media was 15 μM in all the experiments reported here.

The H/D exchange kinetics was investigated with similar incubations of CaM and Ca^{2+} ligand but in a larger volume (e.g., 200 μL). The time for exchange was started when the D_2O (with the same buffer and salt as in H_2O) was added. At each time point, 10 μL of H/D exchange solution was taken out for quenching and analysis. All the incubation and H/D exchange kinetics experiments were conducted at 21.2 ± 0.5 °C. The final concentration of CaM in the H/D exchange solution was 15 μM for all the experiments.

The H/D exchange protocol involves a high D/H ratio in the forward exchange and a high H/D ratio in the back-exchange, and carries the added advantages of in situ desalting. At various points in the titration or kinetic experiments, the D_2O solution containing the exchanging protein, calcium, buffer, and salts was quenched with cold 1 M HCl (to drop the pH to 2.5) and then loaded onto a small C18 guard column, which was cooled at 0 °C with ice and preequilibrated with 100 μL of ice-cold formic acid solution (pH 2.5). The immobilized protein was then back-exchanged and desalted with ice-cold formic acid solution (pH 2.5). The resulting protein was rapidly eluted by using an isocratic flow of solvent with high organic content and at a measured pH of 2.5, and then introduced by ESI into a Finnigan LCQ or Micromass Q-Tof Ultima.

Modeling of the Titration Curve. A description of the modeling can be found in another paper (*83*).

Modeling of Forward H/D Exchange Kinetics. The H/D exchange data were fitted with a three-group kinetic model in which all exchangeable amide hydrogens (from the sequence) were separated into fast, intermediate, and slow groups on the basis of their average H/D exchange rates. For each group of amide hydrogens, the deuterium exchange reaction is assumed to obey pseudo-first-order kinetics (eq 1) with an average rate constant of k_i. $D(H_i,k_i,t)$ is the

$$D(H_i,k_i,t) = aH_i(1 - e^{-k_i t}) \quad (1)$$

deuterium uptake for each group of hydrogens measured in the experiment. H_i is the number of exchangeable hydrogens in each group. The percentage of D_2O in the H/D exchange solution was represented as a ($a = 0.99$ for the experiments reported here), and t is time in minutes.

Therefore, the total number of exchangeable amide hydrogens ($H_{total} = 145$ for CaM on the basis of the sequence) equals the sum of the number of exchangeable hydrogens in each group ($i = 1$, fast; $i = 2$, intermediate; $i = 3$, slow):

$$H_{total} = \sum_{i=1}^{3} H_i = 145 \quad (2)$$

All rate constants were constrained by the following relationship:

$$k_1 > k_2 > k_3 > 0 \quad (3)$$

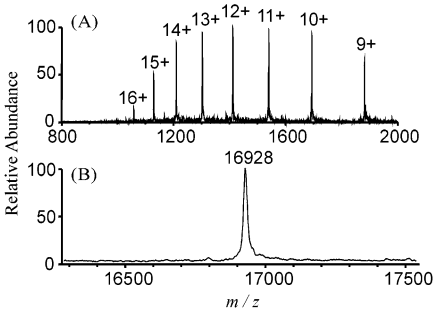

FIGURE 1: Typical ESI mass spectra from LCQ for porcine calmodulin after H/D exchange for 1 h (A) before and (B) after deconvolution (MW of apo-CaM without H/D exchange 16790, [CaM] = 15 μM, [Ca^{2+}] = 20 μM, H/D exchange in 99% D_2O with 20 mM NH_4OAc, quenching, desalting, eluting at pH 2.5).

The analysis component solved for selected underlying unknown parameters (k_i and H_i) in a sequence of trials. In each trial, the search algorithm postulated a set of average rate constants (k_1, k_2, k_3) and the number of exchangeable amide hydrogens in each group (H_1, H_2, H_3). The residuals of the trial are the differences between the experimentally measured overall shift in mass ($A_{j,l}$, with $l > 0$) between the protonated and deuterated protein. $A_{j,0}$ are the experimental times. The error of the trial ϵ was measured as the root mean square (RMS) of the residuals:

$$\epsilon = [(\sum_{j=0}^{M-1} [A_{j,1} - D(H_1,k_1,A_{j,0}) - D(H_2,k_2,A_{j,0}) - D(H_{total} - H_2 - H_1,k_3,A_{j,0})]^2)/M]^{1/2} \quad (4)$$

M is the total number of time points for each set of kinetic experiments. The search was conducted with the "Minimize" function in Mathcad to minimize the trial error. The initial values for the search were guesses often informed by observation of the experimental data. If data were available from more than one replicate of the titration experiment, each set of kinetic data was fitted separately. The results were then averaged, and standard or average deviations were reported.

RESULTS AND DISCUSSION

Advantages of the Improved H/D Exchange Protocol. We improved the H/D exchange protocol described in our first report (*23*) and realized several advantages in sensitivity and mass resolving power, as can be seen by typical mass spectral data shown in Figure 1. First, we are now able to do the exchange in solutions containing high concentrations of salt and buffer. Because the pH is decreased and metal cations are removed prior to MS analysis, all forms of the protein revert back to the apo state, giving minimal signal dispersion and a good signal-to-noise ratio. Concentrating the protein on a guard column prior to introduction into the mass spectrometer allows us to use lower amounts than with our previous protocol. By increasing the volume of the exchange solution injected onto column, we can obtain ESI mass spectra of the protein exchanged at low concentration (e.g., 10^{-8} M) with quality similar to that at high concentration (10^{-5} M). Normally, 10 pmol of protein per injection is sufficient for good ESI-MS analysis. This new H/D exchange protocol also improves the mass resolving power because

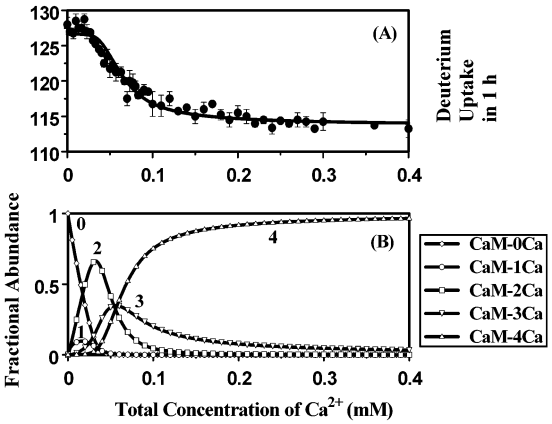

FIGURE 2: (A) Ca titration for 15 μM porcine calmodulin in 50 mM HEPES (pH 7.4, $T = 21.5$ °C, 90% D_2O). Error bars are based on the deviation from two sets of Q-TOF data. The solid curve is the best fit for the average data using the four-parameter model. (B) Species fraction as a function of total [Ca^{2+}] for CaM interacting with four Ca^{2+}.

metal ion interference is removed. By maintaining a high D:H ratio (99:1 or 90:1) in the forward exchange and a high H:D ratio (>100:1) in the back-exchange, we find a narrow isotope distribution and concomitant improved mass resolving power (Figure 1). By manually desalting on the guard column and eluting rapidly with a high concentration of organic in the LC solvent, we maintain the time between quenching and MS analysis to be less than 1 min, minimizing back-exchange. For example, when we applied this protocol to the small peptide melittin, we found fully deuterated peptide ions, indicating that the back-exchange of amide deuterons was nearly negligible.

Ca^{2+} Titration of Calmodulin. To explore the Ca^{2+} binding and the resulting conformational changes to CaM, we applied PLIMSTEX (*81*) to CaM−Ca interactions. A plot of the mass differences between the deuterated and nondeuterated CaM (defined as deuterium uptake) as a function of the total concentration of Ca^{2+} (Figure 2A) forms the titration curve. To understand the shape of the titration curve, we calculated, using previously reported macroscopic binding constants (*38*), the binding fractions of Ca^{2+}-bound species of CaM, CaM−*x*Ca ($x = 1-4$) as a function of the total concentration of Ca^{2+} (the resulting graph is very similar to that in Figure 2B). Given that the titration data are nearly the mirror image of the CaM−4Ca species fraction (compare panels A and B-4 of Figure 2), we conclude that the formation of CaM−4Ca plays the major role in the determination of the general shape of the CaM−Ca titration curve. The similarity suggests that we could fit the titration data by using a 1:4 protein−Ca^{2+} sequential-binding model, assuming that the change in H/D exchange behavior is due principally to an increase in protection afforded in the CaM−4Ca form. On the basis of this assumption, we built a four-parameter (β_3, β_4, ΔD_4 and D_0) fitting program for modeling the titration data, where β_i ($i = 1-4$) refers to the overall equilibrium binding constants, ΔD_4 is the change in the extent of exchange as a result of binding four Ca^{2+} ions compared to that of apo-CaM, and D_0 is the extent of exchange of the apo-CaM (*83*). Because the binding of the fourth, and possibly the third, Ca^{2+} is important in changing the conformation of CaM, only β_3 and β_4 were searched in the model [for the calculation of K_3, we took β_2 from the literature (*38*)]. To account for any experimental errors in measuring the deuterium uptake of apo-CaM, we also took D_0 as a variable (search parameter). The fitted curve for the Ca^{2+} titration of CaM in 50 mM HEPES buffer is shown as a solid line (Figure 2A). One hour was an appropriate time to measure the extent of exchange because it had reached the steady state with a significant difference at that time in the extent of exchange between apo- and holo-CaM. With the first additions of Ca^{2+}, the extent of H/D exchange either stayed constant or increased slightly, indicating no gain and perhaps a slight loss of protection for CaM with binding of one Ca^{2+}. As more Ca^{2+} was added, the extent of H/D exchange dropped dramatically and leveled off when the protein was saturated with Ca^{2+}.

The interactions with the first one or two calcium ions do not perturb CaM's conformation in a significant way. Therefore, we could not obtain K_1 and K_2 from the titration, and we took these constants from published florescence studies that were done under comparable pH and ionic strength (*31*). Modeling the titration curve gave β_3 and β_4, from which we could calculate K_3 and K_4. The two literature sequential binding constants are $K_1 = 2.51 \times 10^5\ M^{-1}$ and $K_2 = 5.01 \times 10^6\ M^{-1}$, whereas $K_3 = 7.12 \times 10^4\ M^{-1}$ and $K_4 = 1.10 \times 10^5\ M^{-1}$ come from PLIMSTEX. The binding polynomial shows that apo-CaM (CaM−0Ca) disappears quickly with an increase of total [Ca^{2+}]. CaM−1Ca and CaM−3Ca never become abundant but give way quickly to CaM−2Ca and CaM−4Ca, respectively, substantiating cooperativity in the binding. The major changes in fractional species occur between the formation of CaM−2Ca and that of CaM−4Ca, which is mirrored by the titration curve, where the greatest difference in exchange also occurs as CaM−2Ca goes to CaM−4Ca. After the fourth Ca^{2+} is bound, the extent of exchange drops to its lowest level and becomes nearly constant. None of the nonspecific binding of more than four Ca^{2+} ions is registered in the titration, indicating that if further binding to Ca^{2+} occurs, it does not cause any significant conformational changes in the protein.

The fractional-species calculation of the Ca^{2+}-bound CaM species, CaM−*x*Ca ($x = 0-4$) is based on the macroscopic binding constants K_3 and K_4 extracted from our titration data and the K_1 and K_2 from the literature (Figure 2B). The curves are nearly identical when K_3 and K_4 are taken from the literature.

The stepwise macroscopic binding constants (K_i), which are readily calculated from β_i, compare favorably with the literature values (Table 1). (The standard deviations for the various search parameters are based on two independent titrations.) PLIMSTEX gives the macroscopic binding constants (K_3 *and* K_4). The average affinity for binding the last two Ca^{2+} ions [$(K_3K_4)^{1/2}$] agrees with literature values (*31*) within a factor of 3. $4K_4/K_3$ (*38*) is much greater than 1, indicating that there is positive cooperativity for binding of the last two Ca^{2+} ions. When the input values of K_1 *and* K_2 for the four-parameter modeling procedure were artificially increased or decreased by a factor of 8, both β_3 and β_4 predicted by four-parameter fitting changed, but the calculated K_4 remained nearly constant (within a factor of 1.2) and K_3 only varied within a factor of 2. Thus, K_3 *and* K_4 calculated from the curve fitting are relatively insensitive to the choice of K_1 *and* K_2, which could be estimated for a new, unknown protein or taken from the literature. The

Table 1: Binding Affinities Obtained from Ca Titrations of Porcine Calmodulin[a]

param	4-parameter fit model (β_3, β_4, D_0, ΔD_4)	7-parameter fit model (β_3, β_4, D_0, ΔD_1, ΔD_2, ΔD_3, ΔD_4)	lit. value (*31*)
β_3 (10^{16} M^{-1})	9 ± 2	2.5 ± 0.6	5.0
β_4 (10^{21} M^{-1})	10 ± 3	3 ± 1	16
K_3 (10^4 M^{-1})	7 ± 2	2.0 ± 0.5	4.0
K_4 (10^5 M^{-1})	1.1 ± 0.4	1.2 ± 0.5	3.2
$(K_3K_4)^{1/2}$ (10^4 M^{-1})	9 ± 1	5.0 ± 0.8	11
D_0	126.7 ± 0.3	128.4 ± 0.8	
ΔD_1	0	-1 ± 9	
ΔD_2	0	3.5 ± 0.7	
ΔD_3	0	0.5 ± 1.3	
ΔD_4	12.6 ± 0.3	14.8 ± 0.7	
RMS	1.0	0.8	

[a] [CaM] = 15 μM, in 50 mM HEPES, 90% D_2O, apparent pH 7.4, T = 21.5 °C.

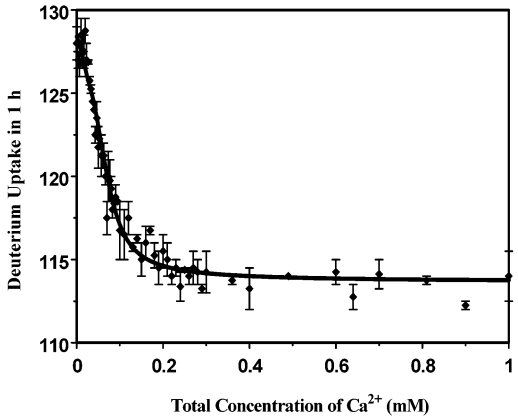

FIGURE 3: Seven-parameter curve fit for 15 μM porcine calmodulin titrated with Ca^{2+} in 50 mM HEPES (same experimental data as in Figure 2).

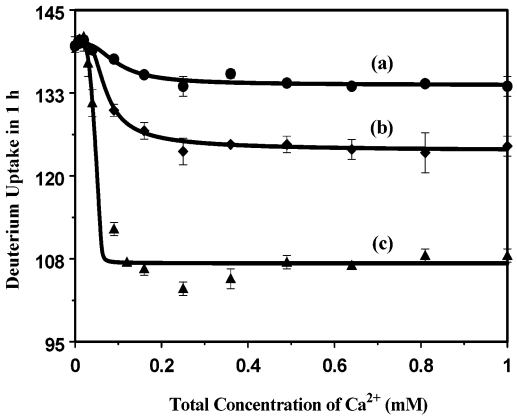

FIGURE 4: Ca titration of 15 μM porcine CaM in three different media (99% D_2O): (a) 50 mM HEPES/0.1 M KCl, apparent pH 7.4; (b) 50 mM HEPES, apparent pH 7.4; (c) 2 mM NH_4OAc, apparent pH 7.0. Error bars were based on two sets of LCQ titration data. Solid curves are from the four-parameter model and are the best fit for the average data.

Table 2: Binding Affinity and Changes in H/D Exchange for Porcine Calmodulin Titrated with Ca^{2+} in Different Media[a]

M^+ added	rel β_3[b]	rel β_4[c]	rel K_3K_4[d]	ΔD_4[e]	D_0[f]
Na^+ [g]	0.001	0.003	0.05	4.2	139.2
Li^+ [g]	0.001	0.004	0.06	6	139.6
K^+ [g]	0.005	0.006	0.08	6	139.9
NH_4^+ [g]	0.002	0.001	0.01	8.9	139.1
Cs^+ [g]	0.002	0.002	0.03	9	138.6
50 mM HEPES[h]	1[i]	1[j]	1[k]	16	140.2
2 mM NH_4OAc[h]	8×10^5	4×10^5	1.4×10^3	34	140.4

[a] Based on duplicate LCQ titration data for each experiment, av RMS = 0.8 u. [b] Av rel dev = 8. [c,d] Av rel dev = 2. [e] Av dev = 1 u. [f] Av dev = 0.4 u. [g] In 100 mM M^+/50 mM HEPES (pH 7.4). [h] No other salts. [i] $\beta_3 = 1 \times 10^{17}$ M^{-3}. [j] $\beta_4 = 6 \times 10^{21}$ M^{-4}. [k] $K_3K_4 = 5 \times 10^9$ M^{-2}.

goodness of the fit was measured as the RMS of the error between the predicted and the experimentally measured deuterium shift; the RMS for the simple four-parameter fitting is 1.0 u.

The positive ΔD_4, which indicates that binding four Ca^{2+} ions to the protein causes ~13 amide linkages to be more protected against forward H/D exchange compared to those of apo-CaM, should be viewed as a quantitative measure of the conformational change. The gain in protection is due to either a direct ligand interaction or a global conformational change, or both. Ca^{2+}-loaded CaM apparently has a more compact structure than apo-CaM, making the protein less solvent-accessible. This interpretation is consistent with that for gel-filtration results in which the Stokes radius of CaM decreased when CaM was saturated with Ca^{2+} (*25*).

The main drawback of the four-parameter model is that it did not fit well the initial part of the titration curve because we ignored contributions to exchange by all Ca^{2+}-bound species other than CaM−4Ca. To better correlate the data, we implemented a seven-parameter (β_3, β_4, D_0, ΔD_1, ΔD_2, ΔD_3, and ΔD_4) model to take into account any changes in exchange due to all five CaM−xCa (x = 0−4) species (Figure 3). The search results for the seven-parameter fit are also summarized in Table 1. The resulting fit not only accommodates the data early in the titration but also gives a better fit (RMS = 0.8 u). The positive ΔD_2 and ΔD_4 suggest that CaM−2Ca and CaM−4Ca species have more compact structures than does the apo form, whereas the negative ΔD_1 is evidence that the addition of the first Ca^{2+} causes CaM to lose some protection. Because there is positive cooperativity between the first two and the second two Ca^{2+}-binding steps in CaM, causing CaM−1Ca and CaM−3Ca to be the least abundant species during the binding process, the uncertainties for ΔD_1 and ΔD_3 are much greater than for ΔD_2 and ΔD_4, respectively. Although the seven-parameter model gives a better fit than the four-parameter model, especially for the initial part of the titration, it does require a large number of points. Furthermore, it is more sensitive to the experimental errors in the data, and gives less reproducible results for the binding constants. Therefore, we will use the four-parameter model for the analysis of the titration data taken for this study.

Effect of Ionic Strength and Other Cations in CaM−Ca Binding. The improved H/D exchange protocol (particularly the on-line desalting before ESI-MS) allows us to explore Ca^{2+} binding to CaM not only of 15 μM CaM in 2 mM NH_4OAc but also under conditions where the ammonium acetate is replaced with 50 mM HEPES or 50 mM HEPES with 100 mM KCl (Figure 4). The latter conditions are similar to physiological conditions of cellular solutions. The ΔD_4 (Table 2) decreases dramatically from low-ionic-strength media (2 mM NH_4OAc) to high-ionic-strength media (50

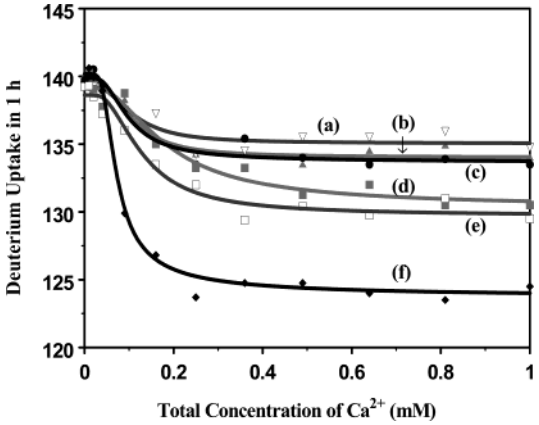

FIGURE 5: Ca titration of 15 μM porcine calmodulin in 50 mM HEPES and 100 mM ionic chlorides: (a) NaCl, open triangles; (b) LiCl, solid triangles; (c) KCl, circles; (d) NH_4Cl, solid squares; (e) CsCl, open squares; (f) no added salt, tilted squares (99% D_2O in H/D exchange media, based on two sets of LCQ data for each titration, giving an average deviation of 0.8 u). Solid curves are the best fits for the average data using the four-parameter model.

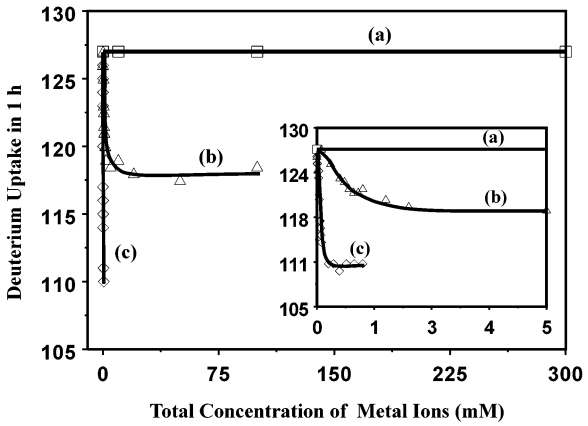

FIGURE 6: Comparison of (a) K^+, (b) Mg^{2+}, and (c) Ca^{2+} titrations of porcine CaM (15 μM CaM, in 50 mM HEPES, apparent pH 7.4, 90% D_2O in H/D exchange media, exchange for 1 h). The solid curves are best fits as judged by the eye.

mM HEPES with 100 mM KCl). The midpoints of the curves shift from low $[Ca^{2+}]_{total}$ to higher $[Ca^{2+}]_{total}$, indicating a reduced Ca^+-binding affinity. The solid lines in Figure 4 are the best-fit curves, and the model gives β_4 and β_3 [β_1 and β_2 were calculated from previously reported K_1 and K_2 values determined at comparable pH and ionic strength (*31*)]. The Ca^{2+}-binding affinity (K_3K_4) decreases by approximately 4 orders of magnitude with an increase in ionic strength and $[K^+]$ from 2 mM to greater than 100 mM, in agreement with results from other methods (*29*, *31*). The agreement supports the validity of the mass spectrometric approach to determining binding affinities. When KCl was replaced by KNO_3 in the H/D exchange media, the new Ca^{2+}-titration curve was nearly identical with the former, indicating that the anion does not play an important role in Ca^{2+} binding to CaM.

To explore the effect of other monovalent cations on Ca^{2+} binding, we carried out similar Ca^{2+} titrations (Figure 5) in 50 mM HEPES with 100 mM LiCl, NaCl, CsCl, or NH_4Cl. Increasing the concentration of these monovalent ions, unlike increasing $[Ca^{2+}]$, does not cause a conformational change in apo-CaM, but does alter the Ca^{2+} binding to CaM (Table 2). At neutral pH, these cations may partially neutralize CaM's negative charges, reducing the electrostatic interactions between the protein and Ca^{2+} and minimizing the conformational change that occurs upon Ca^{2+} binding. The monovalent ions may also change the conformational dynamics of the protein especially in its Ca^{2+}-bound state, allowing the protein to exist longer in the more solvent-accessible state.

The Ca^{2+}-titration curves obtained in the presence of LiCl and NaCl are similar to those obtained in 100 mM KCl. The curves in the presence of CsCl or NH_4Cl, however, fall between those obtained in the presence of HEPES/KCl and in the absence of added salt. Cs^+ and NH_4^+ are less effective in diminishing the conformational change than are the smaller alkaline ions Li^+, Na^+, and K^+, possibly because the larger ionic radii of Cs^+ and NH_4^+ decrease their effective charge.

Haiech and co-workers (*29*) concluded that K^+ binds competitively to the Ca^{2+} site. Two-dimensional ^1H NMR studies of the fragments, however, show that potassium binding does not alter the protein conformation. Alternatively, the effect of K^+ may be due to a screen of electrostatic interactions or a change in activity coefficients (*31*, *38*). To better understand the effect of K^+, a K titration of 15 μM CaM was conducted (Figure 6). The extent of exchange remains constant for increases from 0 to 300 mM in the total K^+ concentration, indicating that no detectable conformational change occurs with added K^+. The repulsive forces of negatively charged amino acids in the Ca^{2+}-binding sites of an EF-hand protein can be overcome by interaction with cations, and highly charged cations would be more effective than singly charged ions. Furthermore, the effective ionic radius of K^+ is larger than that of Ca^{2+} by 38%, suggesting that size also contributes to the selectivity of metal ion binding.

Another important ion in the cell is Mg^{2+}. Although the intracellular Mg^{2+} concentration is approximately 1 mM (*84*), the concentration of monovalent cations is in the 0.1−0.2 M range and the calcium level is as low as 10^{-7} M in the resting cell (but can transiently increase by 2−4 orders of magnitude). When we conducted a Ca^{2+} titration of CaM in 1 mM $MgCl_2$, the affinity and conformational change in the transition between apo-CaM and holo-CaM (data not shown) became smaller compared to that of a Ca titration in the absence of Mg^{2+} (top curve in Figure 4). When CaM is titrated with Mg^{2+} (Figure 6), it does become more protected although the attendant conformational change is much less than that induced by Ca^{2+}. The affinity of CaM for Mg (low millimolar range) is also much smaller than that for Ca^{2+}. The interpretation is consistent with those drawn from other methods (*35*−*37*). Because the effective ionic radius of Mg^{2+} (0.81 Å) is smaller than that of Ca^{2+} (1.06 Å), Mg^{2+} requires a more compact ligand sphere. Unlike Ca^{2+}, which often coordinates with seven oxygen atoms in pentagonal-bipyramidal geometry in Ca^{2+}-binding proteins, Mg^{2+} prefers a coordination number of 6 and more frequently uses nitrogen as a ligand. Thus, the size and coordination environment contribute to the selection of Ca^{2+} over Mg^{2+} in Ca^{2+}-binding sites (*85*). A comparison of K^+, Mg^{2+}, and Ca^{2+} titrations under similar experimental conditions (Figure 6) clearly demonstrates that binding with Ca^{2+} is most favored and induces the largest conformational change whereas K^+ does not cause any detectable change, and Mg^{2+} has intermediate effects. These data indicate that, although Ca^{2+} and Mg^{2+}

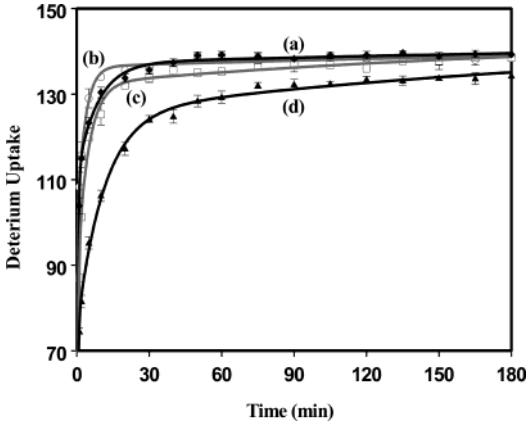

FIGURE 7: Forward H/D exchange kinetics for different CaM−*x*Ca species: (a) CaM−0Ca (apo-CaM), tilted squares; (b) CaM−1Ca, open circles; (c) CaM−2Ca, open squares; (d) CaM−4Ca (holo-CaM), triangles (15 μM CaM, in 50 mM HEPES/0.1 M KCl, apparent pH 7.4, 99% D_2O). The data are the average of at least two runs under identical experimental conditions. The error bars are the average deviation for duplicates or standard deviation for quartets. Solid lines are the best fit for the average data from the three-group kinetics model.

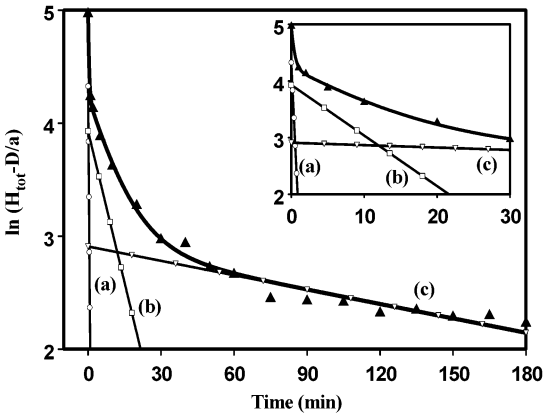

FIGURE 8: Forward H/D exchange kinetics for 15 μM holo-CaM (CaM−4Ca). On the *y*-axis, the natural logarithm of the number of protected hydrogens in the protein is shown as $\ln(H_{total} - D/a)$ where D is the same deuterium uptake as shown in Figure 7 for CaM−4Ca, $H_{total} = 145$ for CaM, and $a = 99\%$. The solid curve is the best fit using the three-group kinetics model. The three lines ($y = -k_i t + \ln H_i$, where k_i and H_i are the rate constant and number of hydrogens for each rate group based on modeling average data from four experiments) are first-order kinetics representations for the three groups of hydrogens: (a) fast group, $y = -2.71919t + \ln(75.7355)$; (b) intermediate group, $y = 0.089341t + \ln(50.9197)$; (c) slow group, $y = -0.004243t + \ln(18.3448)$.

bind specifically with CaM, K^+ interacts via a nonspecific, ionic-strength effect.

Forward H/D Exchange Kinetics for CaM−xCa Fractions. To obtain a better understanding of the titration of CaM with Ca^{2+}, we measured the kinetics of the forward H/D exchange for CaM as a function of $[Ca^{2+}]_{total}$. We chose $[Ca^{2+}]_{total}$ on the basis of the fractional species calculation so as to give maximum concentrations of various CaM−Ca species (e.g., 50 mM HEPES/100 mM KCl; Ca^{2+} concentrations of 0, 0.019, and 0.046 mM give the maximum relative concentrations of apo-CaM, CaM−1Ca, and CaM−2Ca, respectively). The exchange kinetics for holo-CaM was measured at 0.49 mM $[Ca^{2+}]_{total}$, where CaM−4Ca is the predominant species. At each of the Ca^{2+} total concentrations except for 0, there are other CaM−Ca species present (Figure 2B), and the rate constants are averaged over all the species present. Although the uptake of deuterium became nearly constant after 3 h of exchange (Figure 7), there remain a small number of protected amide hydrogens (no less than 6 of 145).

At different pH values and temperatures, the exchange rates of amide hydrogens can vary by several orders of magnitude because changes in the primary sequence, hydrogen bonding, and high-order structure can occur. Several research groups demonstrated that the exchange rates of proteins and peptides occur by multiple pseudo-first-order kinetics (*86*−*89*). Smith's group (*2*) proposed that a plot of deuterium level vs log(time) shows the number of rate constants and hydrogens that exchange with each rate constant. Demmers and co-workers (*88*) separated $\ln(H_{protect})$ vs time plots into multiple straight lines to show composite first-order kinetics and to estimate, from the intercepts, the number of hydrogens associated with each group. The experimental data (triangles in Figure 8) demonstrate that the forward kinetics is more complicated than single pseudo-first-order kinetics. The solid curve in Figure 8 is the best fit from using a three-group, pseudo-first-order kinetics model for the same data shown in the *D* vs *t* plot (triangles in Figure 7). The good fit justifies the separation of all amide hydrogens into fast, intermediate, and slow groups based on the average exchange rates. The three straight lines in Figure 8 are shown using the rate constant (k_i, $i = 1-3$) as the slope and the numbers of hydrogens in each group (H_i, $i = 1-3$) as intercepts. Only the line constructed for the slow group (line c in Figure 8) overlaps the data at long exchange time (i.e., $t > 60$ min). Lines a and b for the intermediate and fast groups do not overlap the experimental data. Thus, an approach (*88*) that aims to fit *graphically* the data into three straight lines will often fail to provide accurate rate constants or extents of exchange for the fast and intermediate groups, because the contribution from one group to the other is ignored in the line fittings. Our model overcomes this disadvantage by using multiexponential nonlinear least-squares regression to fit directly the nonlinear kinetics data.

For better comparison of different Ca^{2+}-binding fractions, we constrained the total number of amide hydrogens ($H_{total} = H_1 + H_2 + H_3$) on the basis of the protein sequence (145 exchangeable amide hydrogens in CaM). All three rate constants (k_1, k_2, k_3) and the number of hydrogens in each group (H_1, H_2, H_3) were treated as positive variables. The solid lines in Figure 7 give the smallest RMS. In other unpublished studies in our laboratory, we found that three classes of rate constants also characterize the kinetics of exchange for rat intestinal fatty acid binding protein (*90*), human ras protein (*91*), and insulin (*92*).

The three rate constants for each CaM−*x*Ca species do not vary significantly under different conditions (Table 3), further supporting the choice of three groups. The average values of the rate constants are ~3.6, ~0.18, and ~0.004 min^{-1}, respectively. The number of hydrogens distributed into these groups, however, varies significantly for different CaM−Ca species (Table 3). Starting with apo-CaM and going to CaM−1Ca, CaM−2Ca, and CaM−4Ca, we find that the number of fast-exchanging hydrogens decreases monotonically from 112 to 75 whereas the number of slow-exchanging hydrogens increases from 6.5 to 18. The number

Table 3: Average Rate Constants and Number of Amide Hydrogens in Each Rate Group for H/D Exchange of Various Porcine CaM−*x*Ca Species[a]

	fast		intermediate		slow	
CaM−*x*Ca species	k_1 (min^{-1}) (~3.6)	H_1	k_2 (min^{-1}) (~0.18)	H_2	k_3 (min^{-1}) (~0.004)	H_3
CaM−0Ca	2.4 ± 0.4	112 ± 2	0.12 ± 0.02	26 ± 2	0.003 ± 0.001	6.5 ± 0.9
CaM−1Ca	7.2 ± 0.6	99 ± 4	0.31 ± 0.02	39 ± 4	0.0024 ± 0.0003	7.1 ± 0.1
CaM−2Ca	2.0 ± 0.2	93 ± 4	0.19 ± 0.03	41 ± 4	0.0051 ± 0.0004	11.7 ± 0.3
CaM−4Ca	2.8 ± 0.2	75 ± 2	0.09 ± 0.01	51 ± 3	0.004 ± 0.001	18 ± 3

[a] Based on at least two sets of Q-TOF kinetics data for each experiment; measured in 100 mM KCl/50 mM HEPES, apparent pH 7.4, $T = 21.2 \pm 0.5$ °C.

of hydrogens in the intermediate group also increased. This distribution is a "signature" of CaM's conformation and should be a useful indicator for other proteins. Fast-exchanging hydrogens are likely to be located on the surface, whereas slow ones are protected by high-order structure, hydrogen bonding, or ligand interactions. More hydrogens shifting from fast to intermediate and slow groups upon Ca^{2+} binding is consistent with a global folding of CaM into a more compact, less solvent-accessible form.

The kinetic results also shed light on the results from the Ca^{2+} titrations. Taking a certain sampling time point (e.g., 60 min) for the titration produces a view that is a weighted superposition of all protein conformation concentrations as a function of metal ion (ligand) concentration. Choosing a different time leads to a view with a different weighting. For example, at 60 min, where the H/D exchange has become nearly constant, the fast and intermediate hydrogens have reached equilibrium, so their weight in the superposition is nearly zero, but those in the slow group are still exchanging, so their weight is dominant. At the start of the titration, apo CaM is the main species, and it has the smallest number of slow-exchanging hydrogens (is least protected). As a result, we see the highest extent of exchange. At the latter stages of the titration, holo-CaM is predominant, has the largest population of slow-exchanging hydrogens among all the CaM−*x*Ca species, and gives the strongest titration signal. The middle part of the titration curve represents a superposition of various CaM−*x*Ca species. Differences in kinetics will give different uptakes of deuterium as a function of sampling time; indeed, if no change in H/D exchange kinetics were observed for different ligand-binding species, the titration curve would be a horizontal line. Thus, PLIMSTEX will work under these conditions only if there is a change in the solvent accessibility as the ligand is added. When there are no differences at long time, methods such as pulsed labeling and rapid mixing may apply because the methods sample fast exchanges ($t_{0.5} < 1$ s).

H/D Exchange Kinetics for Apo- and Holo-CaM in Different Media. The Ca^{2+} titrations in high- vs low-ionic-strength media indicate that the CaM conformational behavior is medium-dependent (Figure 5). Other researchers reported that Ca binding to CaM is insensitive to pH changes in the range of 6.4−8.3 at six different KCl concentrations (*93*). To gain further understanding of the medium effect, we measured forward exchange kinetics for apo- and holo-CaM at low and high ionic strength (Figure 9). The solid lines are the best fits from the three-group kinetic model. Thirteen fast-exchanging amide hydrogens in apo-CaM shift to the intermediate group when the medium is changed from high (HEPES/KCl) to low ionic strength (NH_4OAc), whereas

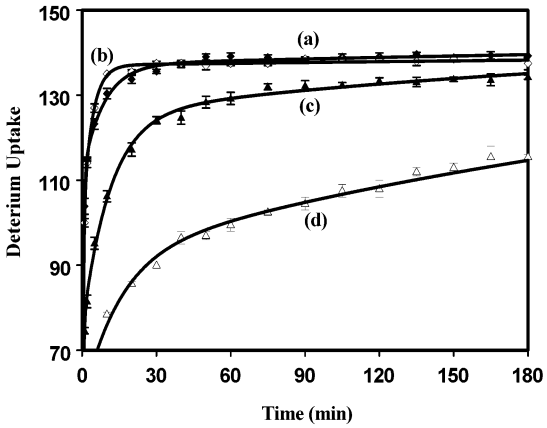

FIGURE 9: Forward H/D exchange kinetics for apo-CaM and holo-CaM in two different media (99% D_2O): (a) apo-CaM in 50 mM HEPES/100 mM KCl, solid tilted squares; (b) apo-CaM in 2 mM NH_4OAc, open tilted squares; (c) holo-CaM in HEPES/KCl, solid triangles; (d) holo-CaM in 2 mM NH_4OAc, open triangles. The error bars are based on at least two sets of Q-TOF data, and the solid curves are the best fits from the three-group kinetics model.

Table 4: Distribution of Rate Constants for H/D Exchange of Apo- and Holo-CaM in Two Media[a]

	no. of exchangeable amide hydrogens		
H/D exchange system	fast ($k_1 \approx 2.3$ min^{-1})	intermediate ($k_2 \approx 0.14$ min^{-1})	slow ($k_3 \approx 0.003$ min^{-1})
apo-CaM in HEPES/KCl	112	26	6.5
apo-CaM in NH_4OAc	99	39	6.5
holo-CaM in HEPES/KCl	75	51	18
holo-CaM in NH_4OAc	59	34.7	51

[a] Based on at least two sets of Q-TOF data for each system. The average deviation for the number of hydrogens in each group is about 2.

the number of hydrogens in the slow group shows little change (Table 4). The outcome is consistent with the observation that the top two curves in Figure 9 for apo-CaM in these two different media are slightly different initially but overlap at longer exchange times ($t > 40$ min). The kinetic results answer the question of why the two Ca^{2+}-titration curves at 1 h (Figure 4) start at the same deuterium level but level off at different extents of exchange for the holo-CaM. There are a smaller number of fast amide hydrogens (59 vs 75) and more slow exchangers (51 vs 18) for the holo-CaM in the low-ionic-strength medium than in the high-ionic-strength medium (Table 4). Therefore, the curve obtained for 2 mM NH_4OAc presents a slower apparent rate and much lower extent of H/D exchange than that obtained when the medium is HEPES/KCl (bottom two curves in Figure 9). The difference in kinetics also shows that, at 1 h,

there is much more protection to exchange at low ionic strength compared to that at high ionic strength.

CONCLUSION

This is the first study in which we applied PLIMSTEX to a biochemical problem. We show that the application of the method yields binding constants for CaM−Ca^{2+} interactions, in both the presence and the absence of other metal ions. When comparisons permit, the PLIMSTEX affinities agree with those in the literature within a factor of 3, substantiating its value as a sensitive and rapid method for affinity determinations. The values of the affinities show clearly that the binding of Ca^{2+} within each domain is cooperative, a fact that was difficult to establish in the early work.

PLIMSTEX also quantitatively reveals the conformational changes associated with the sequential binding of Ca^{2+} with CaM. The binding of the first Ca^{2+} causes a small gain in solvent accessibility, whereas the binding of the fourth Ca^{2+} promotes the largest loss of solvent accessibility (greatest gain in protection). The large ΔD_4 value with respect to ΔD_3, ΔD_2, and ΔD_1 and the striking similarity between the titration curve and the variation of the fraction of CaM−4Ca^{2+} as a function of $[Ca^{2+}]_{total}$ are the evidence that underpins this conclusion.

The affinities of CaM for Ca^{2+} depend on the concentration of other metal ions. In fact, K_3K_4 decreases by approximately 4 orders of magnitude as the ionic strength is increased from the low millimolar range to in excess of 100 mM. PLIMSTEX also shows the quantitative decrease in solvent accessibility in going from apo- to holo-CaM at high vs low ionic strength. Affinities and solvent accessibility associated with Ca^{2+} binding also depend on the nature of the metal. K^+ causes no detectable conformational change, and interactions of Ca^{2+} with CaM in the presence of Li^+, Na^+, and K^+ occur with similar affinity and associated changes in solvent accessibility (the changes are smaller than those in the presence of Cs^+ or NH_4^+). These metal ion effects point to nonspecific rather than competitive binding of alkali-metal ions. Mg^{2+}, however, does bind specifically but competes poorly with Ca^{2+}; its binding causes a smaller change in solvent accessibility, as was established previously.

In addition to equilibrium measurements, mass spectrometry can be used to follow rates of exchange. Modeling the results reveals that the rates fall into three rate classes of fast, intermediate, and slow. The outcome shows that kinetic data provide additional insight into the PLIMSTEX results, and more importantly, the distribution of the number of amides hydrogens in each class appears to offer a "folding signature" for proteins in general.

The data reported here do not allow a distinction between global stabilization afforded by ligand (Ca^{2+}) binding and simple protection at the site of binding. This distinction requires a more incisive look at the protein, which we will achieve by digestion of CaM with pepsin during the course of H/D exchange and measurement of the deuterium content of the resulting peptides.

ACKNOWLEDGMENT

We thank Professor Madeline Shea, Dr. Brenda Sorensen, Dr. Olav Jaren, and Dr. Wendy Van Scyoc for helpful discussions on calmodulin.

REFERENCES

1. Engen, J. R., and Smith, D. L. (2001) *Anal. Chem.*, 256A-265A.
2. Smith, D. L., and Dharmasiri, K. (1998) *NATO ASI Ser., Ser. C. 510*, 45−58.
3. Smith, D. L., Deng, Y., and Zhang, Z. (1997) *J. Am. Soc. Mass Spectrom. 33*, 135−146.
4. Miranker, A., Robinson, C. V., Radford, S. E., and Dobson, C. M. (1996) *FASEB J. 10*, 93−101.
5. Wang, Y., and Gross, M. L. (2002) in *Applied Electrospray Mass Spectrometry* (Ganguly, A. K., Pramanik, B. N., and Gross, M. L., Eds.) Marcel Dekker, New York, p 434.
6. Miranker, A., Robinson, C. V., Radford, S. E., Aplin, R. T., and Dobson, C. M. (1993) *Science 262*, 896−900.
7. Wang, F., Li, W., Emmett, M. R., Marshall, A. G., Corson, D., and Sykes, B. D. (1999) *J. Am. Soc. Mass Spectrom. 10*, 703−710.
8. Neubert, T. A., Walsh, K. A., Hurley, J. B., and Johnson, R. S. (1997) *Protein Sci. 6*, 843−850.
9. Forge, V., Wijesinha, R. T., Balbach, J., Brew, K., Robinson, C. V., Redfield, C., and Dobson, C. M. (1999) *J. Mol. Biol. 288*, 673−688.
10. Klee, C. B. (1988) in *Calmodulin* (Cohen, P., and Klee, C. B., Eds.) Elsevier, Amsterdam.
11. Haiech, J., Kilhofler, M. C., Gerand, D., and Lamaille, J. G. (1982) in *Calmodulin and Intercellular Ca^{2+} Receptors* (Kakiuchi, S., Hidaka, H., and Means, A. R., Eds.) Plenum Press, New York.
12. Yagi, K., Matsuda, S., Nagamoto, H., Mikuni, T., and Yazawa, M. (1982) in *Calmodulin and Intercellular Ca^{2+} Receptors* (Kakiuchi, S., Hidaka, H., and Means, A. R., Eds.) Plenum Press, New York.
13. Rogers, M. S., and Strehler, E. E. (1996) in *Guidebook to the calcium-binding proteins* (Celio, M. R., Pauls, T. L., and Schwaller, B., Eds.) a Sambrook & Tooz Publication at Oxford University Press, Oxford, U.K.
14. Klee, C. B., Crouch, T. H., and Richman, P. G. (1980) *Annu. Rev. Biochem. 49*, 489−515.
15. Vogel, H. J. (1994) *Biochem. Cell Biol. 72*, 357−376.
16. Weinstein, H., and Mehler, E. (1994) *Annu. Rev. Physiol. 56*, 213−236.
17. Crivici, A., and Ikura, M. (1995) *Annu. Rev. Biophys. Biomol. Struct. 24*, 85−116.
18. Cheung, W. Y. (1980) *Science 207*, 19−27.
19. James, P., Vorherr, T., and Carafoli, E. (1995) *Trends Biochem. Sci. 20*, 38−42.
20. Zhang, M., Tanaka, T., and Ikura, M. (1995) *Nat. Struct. Biol. 2*, 758−767.
21. Kuboniwa, H., Tjandra, N., Grzesek, S., Ren, H., Klee, C. B., and Bax, A. (1995) *Nat. Struct. Biol. 2*, 768−776.
22. Finn, B. E., Evanäs, J., Drakenberg, T., Waltho, J. P., Thulin, E., and Forsén, S. (1995) *Nat. Struct. Biol. 2*, 777−783.
23. Nemirovskiy, O., Giblin, D. E., and Gross, M. L. (1999) *J. Am. Soc. Mass Spectrom. 10*, 711−718.
24. Barbato, G., Ikura, M., Kay, L. E., Pastor, R. W., and Bax, A. (1992) *Biochemistry 31*, 5269.
25. Sorensen, B. R., and Shea, M. A. (1996) *Biophys. J. 71*, 3407−3420.
26. Van Scyoc, W. S., and Shea, M. A. (2001) *Protein Sci. 10*, 1758−1768.
27. Sorensen, B. R., and Shea, M. A. (1998) *Biochemistry 37*, 4244−4253.
28. Kilhoffer, M. C., Kubina, M., Travers, F., and Haiech, J. (1992) *Biochemistry 31*, 8098−8106.
29. Haiech, J., Klee, C. B., Demaille, J. G., and Haiech, J. (1981) *Biochemistry 20*, 3890−3897.
30. Martin, S. R., Masina, L., and Bayley, P. M. (2000) *Protein Sci. 9*, 2672−2488.
31. Linse, S., Helmersson, A., and Forsén, S. (1991) *J. Biol. Chem. 266*, 8050−8054.
32. Masino, L., Martin, S. R., and Bayley, P. M. (2000) *Protein Sci. 9*, 1519−1529.
33. Gilli, R., Lafitte, D., Lopez, C., Kilhoffer, M.-C., Makarov, A., Briand, C., and Haiech, J. (1998) *Biochemistry 37*, 5450−5456.
34. Malmendal, A., Linse, S., Evanäs, J., Forsén, S., and Drakenberg, T. (1999) *Biochemistry 38*, 11844−11856.
35. Seaton, B. A., Head, J. F., Lord, R. C., and Petsko, G. A. (1983) *Biochemistry 22*, 973−978.
36. You, G., Buccigross, J. M., and Nelson, D. J. (1990) *J. Inorg. Biochem. 38*, 117−125.

37. Tsai, M.-D., Drakenberg, T., Thulin, E., and Forsén, S. (1987) *Biochemistry 26*, 3635−3643.
38. Forsén, S., Linse, S., Drakenberg, T., Kördel, J., Akke, M., Sellers, P., Johansson, C., Thulin, E., Andersson, I., Brodlin, P., Grundström, T., Skelton, N. J., and Chazin, W. J. (1991) *Ciba Found. Symp. 161* (Protein Conformation), 222−236.
39. Babu, Y. S., Sack, J. S., Greenhough, T. J., Bugg, C. E., Means, A. R., and Cook, W. J. (1985) *Nature 315*, 37−40.
40. Babu, Y. S., Bugg, C. E., and Cook, W. J. (1988) *J. Mol. Biol. 204*, 191−204.
41. Taylor, D. A., Sack, J. S., Maune, J. F., Beckinghan, K., and Quiocho, F. A. (1991) *J. Biol. Chem. 266*, 21375−21380.
42. Chattopadhyaya, R., Meador, W. E., Means, A. R., and Quiocho, F. A. (1992) *J. Mol. Biol. 228*, 1177−1192.
43. Rao, S. T., Wu, S., Statyshur, K. A., Ling, K.-Y., Kung, C., and Sundaralingam, M. (1993) *Protein Sci. 2*, 436−447.
44. Klevit, R. E., Dalgarno, D. C., Levine, B. A., and Williams, R. J. P. (1984) *Eur. J. Biochem. 139*, 109−114.
45. Pedigo, S., and Shea, M. A. (1995) *Biochemistry 34*, 16676−16689.
46. Jaren, O. R., Kranz, J. K., Sorensen, B. R., Wand, A. J., and Shea, M. A. (2002) *Biochemistry 41*, 14158−14166.
47. Starovasnik, M. A., Su, D. R., Beckingham, K., and Klevit, R. E. (1992) *Protein Sci. 1*, 245−253.
48. Martin, S. R., Linse, S., Bayley, P. M., and Forsen, S. (1986) *Eur. J. Biochem. 161*, 595−601.
49. Kilhoffer, M.-C., Demaille, J. G., and Gerard, D. (1981) *Biochemistry 20*, 4407−4414.
50. Watkins, A. N., and Bright, F. V. (1998) *Appl. Spectrosc. 52*, 1447−1456.
51. Doody, M. A., Baker, G. A., Pandey, S., and Bright, F. V. (2000) *Anal. Chem. 72*, 227−233.
52. Shea, M. A., Sorensen, B. R., Pedigo, S., and Verhoeven, A. S. (2000) *Methods Enzymol. 323*, 254−301.
53. Pedigo, S., and Shea, M. A. (1995) *Biochemistry 34*, 1179−1196.
54. Shea, M. A., Verhoeven, A. S., and Pedigo, S. (1996) *Biochemistry 35*, 2943−2957.
55. Klee, C. B. (1977) *Biochemistry 16*, 1017−1024.
56. Crouch, T. H., and Klee, C. B. (1980) *Biochemistry 19*, 3692−3698.
57. Jackson, M., Haris, P. I., and Chapman, D. (1991) *Biochemistry 30*, 9681−9686.
58. Jaren, O. R., Harmon, S., Chen, A. F., and Shea, M. A. (2000) *Biochemistry 39*, 6881−6890.
59. Iida, S., and Potter, J. D. (1986) *J. Biochem. (Tokyo) 99*, 1765−1772.
60. Milos, M., Schaer, J. J., Comte, M., and Cox, J. A. (1986) *Biochemistry 25*, 6279−6287.
61. Protasevich, I., Ranjbar, B., Lobachov, V., Makarov, A., Gilli, R., Briand, C., Lafitte, D., and Haiech, J. (1997) *Biochemistry 36*, 2017−2024.
62. Brokx, R. D., Lopez, M. M., Vogel, H. J., and Makhatadze, G. I. (2001) *J. Biol. Chem. 276*, 14083−14091.
63. Sorensen, B. R., Eppel, J.-T., and Shea, M. A. (2001) *Biochemistry 40*, 896−903.
64. Sorensen, B. R., Faga, L. A., Hultman, R., and Shea, M. A. (2002) *Biochemistry 41*, 15−20.
65. Kupke, D. W., and Dorrier, T. E. (1986) *Biochem. Biophys. Res. Commun. 138*, 199−204.
66. Vainer, H. (1987) *J. Electrochem. Soc. 134*, 1938−1943.
67. Hopkins, H. P., Jr., and Gayden, R. H. (1989) *J. Solution Chem. 18*, 743−757.
68. Doherty-Kirby, A. L., and Lajoie, G. A. (2002) *Methods Mol. Biol. 173* (Calcium-Binding Protein Protocols, Vol. 2), 161−174.
69. Hill, T. J., Lafitte, D., and Derrick, P. J. (2001) in *Electrospray ionization mass spectrometry* (Harding, S. E., and Chowdhry, B. Z., Eds.) pp 311−346, Oxford University Press, Oxford, U.K.
70. Steiner, R. F., Albaugh, S., Fenselau, C., Murphy, C., and Vestling, M. (1991) *Anal. Biochem. 196*, 120−125.
71. Brockerhoff, S. E., Edmonds, C. G., and Davis, T. N. (1992) *Protein Sci. 1*, 504−516.
72. Hu, P., Ye, Q.-Z., and Loo, J. A. (1994) *Anal. Chem. 66*, 4190−4194.
73. Hu, P., and Loo, J. A. (1995) *J. Mass Spectrom. 30*, 1076−1082.
74. Lafitte, D., Capony, J. P., Grassy, G., Haiech, J., and Calas, B. (1995) *Biochemistry 34*, 13825−13832.
75. Nemirovskiy, O. V., Ramanathan, R., and Gross, M. L. (1997) *J. Am. Soc. Mass Spectrom. 8*, 809−812.
76. Veenstra, T. D., Tomlinson, A. J., Benson, L., Kumar, R., and Naylor, S. (1998) *J. Am. Soc. Mass Spectrom. 9*, 580−584.
77. Lafitte, D., Heck, A. J. R., Hill, T. J., Jumel, K., Harding, S. E., and Derrick, P. J. (1999) *Eur. J. Biochem. 261*, 337−344.
78. Hill, T. J., Lafitte, D., Wallace, J. I., Cooper, H. J., Tsvetkov, P. O., and Derrick, P. J. (2000) *Biochemistry 39*, 7284−7290.
79. Gao, J., Yin, D. H., Yao, Y., Sun, H., Qin, Z., Schoneich, C., Williams, T. D., and Squier, T. C. (1998) *Biophys. J. 74*, 1115−1134.
80. Nousiainen, M., Vainiotalo, P., Feng, X., and Derrick, P. J. (2001) *Eur. J. Mass Spectrom. 7*, 393−398.
81. Zhu, M. M., Rempel, D. L., Du, Z., and Gross, M. L. (2003) *J. Am. Chem. Soc. 125*, 5252−5253.
82. Glasoe, P. K., and Long, F. A. (1960) *J. Phys. Chem. 64*, 188−190.
83. Zhu, M. M., Rempel, D. L., and Gross, M. L. (2004) *J. Am. Soc. Mass Spectrom.*, in press.
84. Linse, S., and Forsen, S. (1995) *Adv. Second Messenger Phosphoprotein Res. 30* (Calcium Regulation of Cellular Function), 89−151.
85. Snyder, E. E., Buoscio, B. W., and Falke, J. J. (1990) *Biochemistry 29*, 3937−3943.
86. Zhang, Z., and Smith, D. L. (1993) *Protein Sci. 2*, 522−531.
87. Zhang, Z., Post, C. B., and Smith, D. L. (1996) *Biochemistry 35*, 779.
88. Demmers, J. A. A., Haverkamp, J., Heck, A. J. R., Koeppe, R. E., II, and Killian, J. A. (2000) *PNAS 97*, 3189−3194.
89. Demmers, J. A., van Duijn, E., Haverkamp, J., Greathouse, D. V., Koeppe, R. E. n., Heck, A. J., and Killian, J. A. (2001) *J. Biol. Chem. 276*, 34501−34508.
90. Hodsdon, M. E., Ponder, J. W., and Cistola, D. P. (1996) *J. Mol. Biol. 264*, 585−602.
91. Zhang, J., and Matthews, C. R. (1998) *Biochemistry 37*, 14881−14890.
92. Ramanathan, R., Gross, M. L., Zielinski, W. L., and Layloff, T. P. (1997) *Anal. Chem. 69*, 5142−5145.
93. Svensson, B., Joensson, B., Thulin, E., and Woodward, C. E. (1993) *Biochemistry 32*, 2828−2834.

BI035188O